ACS APPLIED MATERIALS & INTERFACES

Research Article

Cite This: ACS Appl. Mater. Interfaces XXXX, XXX, XXX−XXX

www.acsami.org

Improved Label-Free Identification of Individual Exosome-like Vesicles with Au@Ag Nanoparticles as SERS Substrate

Juan C. Fraire,[†,‡] Stephan Stremersch,[†,‡] Davinia Bouckaert,[§] Tinne Monteyne,[§] Thomas De Beer,[§] Pieter Wuytens,[∥] Riet De Rycke,[⊥,#] Andre G. Skirtach,[∥] Koen Raemdonck,[†] Stefaan De Smedt,[†,▽] and Kevin Braeckmans*[,†,‡,▽]

[†]Laboratory of General Biochemistry and Physical Pharmacy, Faculty of Pharmaceutical Sciences, [‡]Center of Nano- and Biophotonics, Faculty of Pharmaceutical Sciences, [§]Laboratory of Pharmaceutical Process Analytical Technology, [∥]Department of Molecular Biotechnology, Faculty of Bioengineering, [⊥]Center for Inflammation Research, VIB, Ghent, Belgium and Department of Biomedical Molecular Biology, [#]Center for Plant Systems Biology, VIB, Ghent, Belgium and Department of Plant Biotechnology and Bioinformatics, and [▽]Center for Advanced Light Microscopy, Ghent University, 9000 Ghent, Belgium

Supporting Information

ABSTRACT: Exosome-like vesicles (ELVs) are nanovectors released by cells that are endowed with a variety of molecules, including proteins, nucleic acids, and chemicals that reflect the molecular signature of the producing cell. Given their presence in many biofluids, they form an easily accessible biomarker for early disease detection. Previously we demonstrated the possibility of identifying individual ELVs by analyzing their molecular signatures with surface-enhanced Raman scattering (SERS) after functionalization of ELVs with 4-(dimethylamino)pyridine (DMAP)-stabilized gold nanoparticles (AuNP). Although this strategy was capable of distinguishing ELVs from different cellular origins, the quality of the SERS spectra was suboptimal due to high background coming from the DMAP stabilizing molecules at the AuNP surface. In this study we demonstrate that it is possible to eliminate interfering SERS signals from stabilizing molecules at the AuNP surface by overgrowing *in situ* the ELV-attached AuNPs with a silver layer so as to form a core−shell nanoparticle (Au@AgNPs) directly at the ELV surface. As such it represents the first known strategy to generate clear SERS spectral fingerprints of delicate biological structures without interference of linker molecules that are needed to ensure colloidal stability of the plasmonic NP and to allow them to associate to the ELV surface. This new strategy using core−shell plasmonic NPs as SERS substrate showed higher near-field enhancements than previous approaches, which resulted in SERS spectra with improved signal-to-noise ratio. This allowed us to discriminate individual vesicles derived from B16F10 melanoma cells and red blood cells (RBC) with an unprecedented sensitivity and specificity >90%. Importantly, thanks to the higher near field enhancement the acquisition time could be reduced by 20-fold in comparison to previously reported strategies, paving the way toward high-throughput label-free single ELV identification.

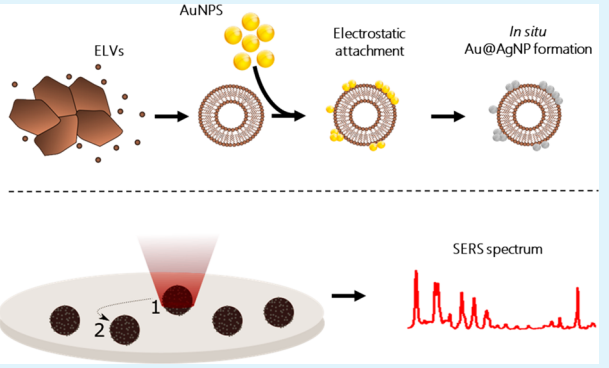

KEYWORDS: *extracellular vesicles, core−shell plasmonic nanoparticles, SERS, biosensor, diagnostics*

INTRODUCTION

Exosome-like vesicles (ELVs) are nanometer-sized vesicular structures composed of an aqueous core enveloped with a lipid membrane containing nucleic acids and soluble and membrane-associated peptides.[1] ELVs originate from the endosomal pathway and are formed by the inward budding of late endosomes and subsequent fusion of the resulting multivesicular bodies with the cell membrane. Increasing evidence demonstrates their involvement in intercellular communication and removal of waste products out of the cell. Upon release of these vesicles by cells in the body, a large fraction end up in the different body fluids, which makes them easily accessible for detection.[2] As these vesicles contain molecules derived directly from the parent cell, they have been recognized as candidate biomarkers for early detection and monitoring of various diseases including cancer.[3,4]

In recent years, the observed difference in omics profiles between extracellular vesicles from healthy versus diseased cells has led to the development of various diagnostic assays.[5−9] The most common method used for ELV detection is ELISA, which requires relatively large volumes of highly concentrated samples and the use of selective antibodies or labels against

Received: July 1, 2019
Accepted: October 4, 2019
Published: October 4, 2019

DOI: 10.1021/acsami.9b11473
ACS Appl. Mater. Interfaces XXXX, XXX, XXX−XXX

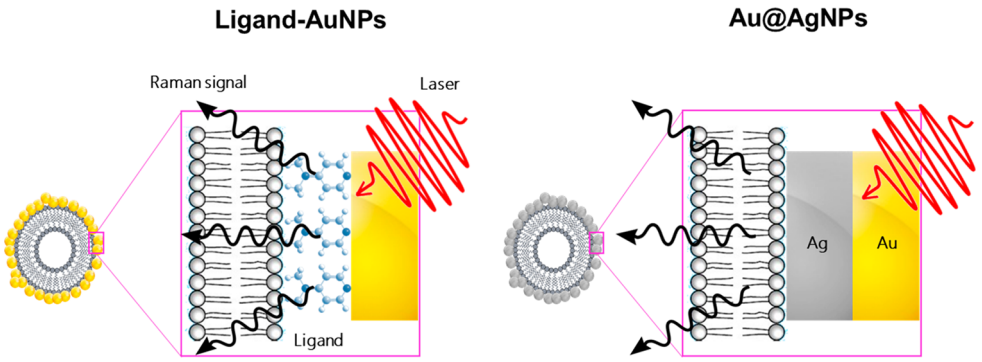

Figure 1. *In situ* Au@AgNP formation as a strategy to obtain a clear spectral fingerprint of individual ELVs. Schematic representation of ligand-stabilized AuNP attached to the outer ELV surface and Au@AgNP in which the ligand coating is replaced by an outer silver layer.

previously identified biomarkers on the ELV membrane.[10] The development of optical biosensing methods, in particular plasmonic systems, allowed to develop surface plasmon resonance (SPR) sensors, overcoming the sensitivity of ELISA at least by 2 orders of magnitude.[11] Despite the improvements in detection sensitivity, this approach still relies on antibody-mediated detection of previously determined ELV surface markers. Therefore, quite some effort has gone into developing new label-free and nondestructive methodologies for ELV detection. A particularly promising technique in this regard is surface-enhanced Raman spectroscopy (SERS), which makes use of plasmonic properties to obtain information about the vibrational modes of molecules with high sensitivity.[12−14] SERS is a plasmonic phenomenon associated with the collective oscillation of the conductive electrons of noble metal nanoparticles (NPs), known as localized surface plasmon resonance (LSPR). LSPR excitation induces an enhanced electromagnetic field surrounding the metallic nanoparticle (near-field) with a spatial distribution that depends for a given metallic nanostructure on its geometry, its orientation with respect to the incident polarization, illumination wavelength, and dielectric environment.[15,16] When a Raman-active molecule is located within the enhanced electromagnetic field, the number of inelastically scattered photons containing information about the molecular composition of the sample is dramatically increased by several orders of magnitude. In this way, SERS substantially enhances the signal-to-noise ratio of Raman spectra, enabling the detection of very few molecules or even single molecules on or near plasmonic nanoparticles.[17] Currently, most SERS-based diagnostic approaches for ELVs focus on identifying spectral features that can be attributed to specific macromolecules that are linked to the parent cells.[18−22] So far, however, most of these analyses were performed on the ensemble ELV population, which contains vesicles of many types of cells when isolated from body fluids. This makes detection of low abundant subpopulations of exosomes that are linked to the disease state of interest challenging, especially when the aim is to detect the disease in an early stage.

In previous work we reported on a new approach to identify individual ELVs by SERS after functionalization with plasmonic gold nanoparticles (AuNPs) on the outer surface of the vesicles, as schematically depicted on the left-hand side in Figure 1.[13] While we demonstrated successful identification and classification of ELVs according to their originating parent cells, the quality of the SERS spectra was substantially limited by the intense signal coming from the surface ligand of the AuNP (4-(dimethylamino)pyridine (DMAP)). Interfering SERS signals from stabilizing molecules at plasmonic surfaces complicates the analysis of spectral fingerprints of analytes considerably since these stabilizing molecules are closest to the AuNP surface, being the region of highest near field enhancement. At the same time the stabilizing molecules cannot easily be left out as they are needed for colloidal stability and binding to the ELV surface. In the here presented work, we aimed to develop a strategy to effectively remove interfering signals from stabilizing molecules at the AuNP surface so as to improve SERS-based classification of individual ELVs. To this end, we show that it is possible to overgrow *in situ* a silver layer on the ELV-attached AuNPs, so as to form Au@AgNPs directly at the ELV surface without destroying the delicate ELV. The expected benefits are twofold. Apart from generating cleaner and more informative spectra, it will generate higher near-field enhancements (SERS spectra of better signal-to-noise quality) of the vesicle surface, which is now in direct contact with the metal surface (Figure 1). This hypothesis was first verified theoretically through simulations and subsequently confirmed experimentally. As such it represents the first known strategy to generate clear SERS spectral fingerprints of individual ELVs without interference of the surface ligands that are needed for colloidal stability and to initially attach the plasmonic NPs to those structures. As a proof-of-concept of the detection potential of this approach, we show that vesicles derived from B16F10 melanoma cells can be successfully discriminated from red blood cell (RBC)-derived vesicles. PLS-DA analysis of the resulting Raman spectra reached an unprecedented sensitivity and specificity above 90% for both types of ELVs. Combined with a 20-fold reduction in measurement time, the presented approach provides an important and essential step toward making high-throughput label-free identification of single ELVs a reality.

MATERIALS AND METHODS

Materials. The following materials were used as obtained: $HAuCl_4$ (Aldrich), Ag_2SO_4 (Aldrich), sodium citrate (Sigma-Aldrich), sodium ascorbate (Aldrich), tetraoctylammonium (Aldrich), 4-(dimethylamino)pyridine (DMAP, Aldrich), toluene (Sigma-Aldrich), sulfuric acid (Sigma), sodium hydroxide (Sigma), iodixanol (Sigma-Aldrich), phosphate buffered saline PBS (Invitrogen), fetal bovine serum (FBS, Hyclone), penicillin (Invitrogen), streptomycin (Invitrogen), Dulbecco's modified eagle medium (Invitrogen), sodium pyruvate (Invitrogen), CaF_2 Raman grade slides (Crystran Ltd.), and a Beckman L8-70M ultracentrifuge equipped with a SW55t1 rotor (Beckman instruments).

DOI: 10.1021/acsami.9b11473
ACS Appl. Mater. Interfaces XXXX, XXX, XXX−XXX

Nanoparticle Synthesis. The synthesis of gold nanoparticles was performed using the method described by Gittins and Caruso.[25] Briefly, $HAuCl_4$ aqueous solution was added to a tetraoctylammonium bromide in toluene solution under gentle stirring. Next, $NaBH_4$ was added to the mixture. After 30 min the toluene phase was separated from the aqueous phase and washed three times using sulfuric acid, NaOH, and ultrapure water. Equal volumes of the AuNP in toluene solution and an aqueous DMAP solution were mixed and left to equilibrate for 1 h. During this period the AuNPs transfer from the organic toluene phase to the aqueous phase, concomitantly exchanging the tetraoctylammonium bromide coat for a DMAP coating. Finally, the aqueous phase, containing the AuNP coated with DMAP, is separated from the toluene phase. The morphological characterization of the DMAP-coated AuNPs was performed by combining UV−vis spectroscopy (Nanodrop 2000c; Thermo Scientific), dynamic light scattering (DLS), and electrodynamic modeling using Mie theory. The overall results after combining all of these different techniques and modeling indicate that the average diameter was 7 nm with a zeta potential of +18.5 mV. The concentration was estimated to be around 1.9×10^{15} NP/mLby using the experimental extinction intensities at the maximum wavelength and Mie theory calculations of the extinction cross section for spherical particles with the corresponding diameter (determined by DLS).

Nanoparticle Coating of ELVs. ELVs were mixed with DMAP−AuNP at different AuNP:vesicle ratios by mixing equal volumes using a pipet as described previously.[13] After 10 min incubation at room temperature, the samples were diluted in ultrapure water and further analyzed. Changes in the zeta potential of ELVs as a function of the AuNP:vesicle ratio were measured. 100% coating of the ELV was considered to be the ratio at which, theoretically, the AuNPs added are sufficient to fully cover the total surface of ELVs present. This was calculated as previously reported.[13] Isolated ELVs were mixed with DMAP−AuNP using the same experimental conditions as previously reported (i.e., for B16F10-derived ELVs 100% coating corresponds with 800 AuNPs added per vesicle and for RBC-derived ELVs 100% coating corresponds with 1200 AuNPs per vesicle). Lower cover percentages were calculated according to these values.

Silver Coating of AuNPs. The generation of a silver layer onto the AuNPs was achieved by following the indications of previously reported procedures.[26] The optimal conditions were found to be the addition of 100 μL of Ag^+ (0.03 M) and 200 μL of sodium ascorbate (0.01 M) per 10 mL of AuNPs (1.9×10^{15} NP/mL) and let it react for 30 min at pH = 8−9 (see Figure 4A). The amounts or coating agents used were adjusted as a function of the final concentration of AuNPs used to functionalize the ELVs considering the loading capacity for achieving colloidal stability (determined previously by DLS).

Cell Culturing and ELV Isolation. B16F10 melanoma cells (ATCC CRL-6475) were cultured in Dulbecco's Modified Eagle Medium (Invitrogen), supplemented with L-glutamine (2×10^{-3} M), 10% heat-inactivated FBS, sodium pyruvate (1×10^{-3} M), penicillin (100 U/mL), and streptomycin (100 μg/mL) at 37 °C in a humidified atmosphere containing 5% CO_2. For the purification of ELVs, cells were first washed with phosphate buffered saline, and the cell medium was replaced with vesicle-depleted medium. The latter was prepared by ultrafiltration of a complete cell culture medium through a 300 kDa filter (Millipore) using an Amicon stirred cell setup (Millipore) under 3 bar nitrogen pressure to remove bovine vesicles. Cells were incubated for 24 h, after which the conditioned cell medium was harvested for vesicle purification.

RBCs were isolated out of the blood from a healthy volunteer as described previously[27] with minor modifications. Briefly, blood was collected in K_2EDTA-coated tubes (Venosafe) and spun at 1500*g* for 15 min (Heraeus Multifuge 1S-R) within 10 min after blood collection. RBCs were retained, washed twice, and suspended in Ringer buffer for 2 days at 37 °C while shaking.

ELVs produced by B16F10 melanoma cells and RBCs were purified from a conditioned cell medium or Ringer buffer, respectively, by differential centrifugation followed by density gradient UC as previously described.[13] Briefly, the conditioned cell medium or Ringer buffer was centrifuged for 10 min at 3000*g*. Next, the supernatant was concentrated by ultrafiltration. The concentrated sample was centrifuged at 10000*g* for 10 min with an SW55ti rotor, and the supernatant was placed on top of an iodixanol-based density gradient. The gradient was produced according to the manufacturer's instructions. Briefly, 1 mL of different iodixanol dilutions (12.5%, 25%, 37.5%, and 50%) was carefully laid underneath one another by using a 21G needle. The samples were then centrifuged at 150000*g* for 15 h. Next, the gradient was fractionated per 0.5 mL and centrifuged again at 150000*g* for 150 min. Finally, the pellet was washed one more time and suspended in ultrapure water. The fraction containing the ELV associated proteins was used for further characterization and Raman spectroscopy experiments. The vesicles in this fraction are termed ELVs throughout the article. Extensive characterization of the obtained ELVs using the described isolation strategy can be found in Stremersch et al.[26] Briefly, with respect to ELV purity, in this work we started from ELVs isolated by using density gradient ultracentrifugation, which is a very stringent purification method that minimizes the presence of nonvesicular components such as protein and RNA complexes.[27] In addition, a very elaborate profiling of ELVs isolated with this purification strategy has been done by our group which was submitted to the EV-track database (EV-track ID: EV160001) receiving a very high score of 87%.[26]

Concentration, Size, and Zeta-Potential Measurements. The concentration of purified ELVs was determined by light scattering based single particle tracking using a NanoSight LM10 instrument (Malvern Instruments Ltd.) equipped with a 405 nm laser. Prior to analysis, the concentrated vesicles were diluted in HEPES buffer (pH 7.4; 20×10^{-3} M) to obtain a concentration in the range of $(1.0-9.0) \times 10^8$ vesicles/mL to guarantee reliable measurements. Movies of 60 s were recorded and analyzed with the NTA Analytical Software version 2.3 (Malvern Instruments Ltd.). The size and zeta-potential of ELVs and metal-functionalized ELVs were measured by dynamic light scattering using a Zetasizer Nano ZS (Malvern Instruments Ltd.), equipped with Dispersion Technology software.

SERS Measurements. Isolated ELVs were mixed with DMAP−AuNP by using the same experimental conditions as described above. When indicated, the silver coating was applied. Next, samples were diluted in ultrapure water to $\leq 5 \times 10^7$ ELVs/μL to facilitate the recording of single vesicles. A droplet (60 μL) of the diluted sample was placed on a CaF_2 substrate. SERS spectra were acquired on a WITec Alpha 300 R+ confocal Raman microscope equipped with a −65 °C cooled CCD camera (Andor iDus 401 BR-DD) and a 785 nm laser (Toptica XTRA II) and collected through a water dipping objective (Zeiss 63×/1.0 W Plan Apochromat) with a 500 ms integration time and 15 mW incident power (in our previously reported strategy the integration time was 20-fold higher = 10 s).[13] The 785 nm laser was chosen to limit photodegradation and autofluorescence.[28,29] All spectra were recorded at different locations in the sample. The presence of a metal-functionalized ELV in the focal volume was confirmed by light scattering.

Analysis of SERS Spectra. For statistical analysis, the obtained spectra were preprocessed as described previously.[30] To assess the ability of Raman spectroscopy to discriminate RBC- and B16F10 melanoma-derived ELVs, a partial least-squares discriminant analysis (PLS-DA) was performed by using PLS_Toolbox from eigenvector Research, Inc. in MATLAB. A detailed description of the PLS-DA method can be found in the Supporting Information.

Transmission Electron Microscopy (TEM). TEM images were obtained at the VIB-UGent Transmission Electron Microscopy-Core facility by using a JEM 1400plus transmission electron microscope (JEOL, Tokyo, Japan) operating at 80 kV. Nanoparticle samples were prepared by adding one drop (~50 μL) of the colloidal dispersion onto Formvar/C-coated hexagonal copper grids (EMS G200H-Cu) for 20 min and washed five times in double-distilled H_2O. To visualize the ELV's or NP-functionalized ELVs, the grids were glow discharged for 10 s and placed on top of the drop (~50 μL) for 20 min, coated side of the grid down. The grids were stained with 1% (w/v) uranyl

DOI: 10.1021/acsami.9b11473
ACS Appl. Mater. Interfaces XXXX, XXX, XXX−XXX

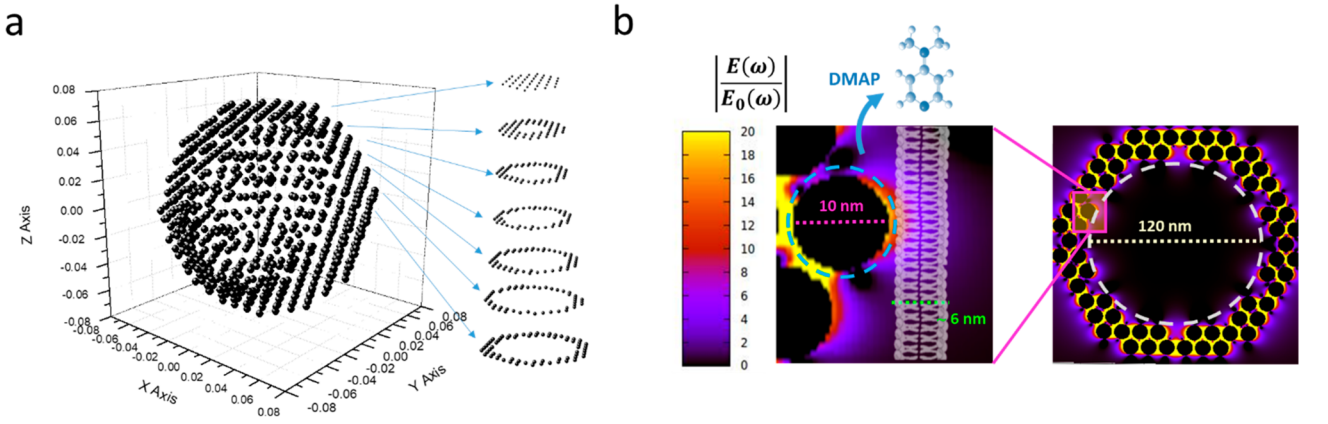

Figure 2. Near-field optical characterization of AuNP-coated ELVs. (a) Spatial distribution of AuNPs arranged in close packing around a 120 nm in diameter sphere (ELV). The gap between NPs was 2 times the length of a DMAP molecule (gap = 1.3 nm). The complete distribution of particles can be separated in planes, as shown in the right inset, for the near-field calculations. (b) Spatial distribution of *E*-field enhancement at 785 nm at the middle plane of the vesicle. The zoom-in (depicted as the pink box) shows the *E*-field enhancement around a single AuNP attached to the vesicle surface. The blue dashed circle indicates the region where DMAP molecules are present at the AuNP surface. It shows that those molecules experience a much stronger *E*-field enhancement as compared to the vesicle surface.

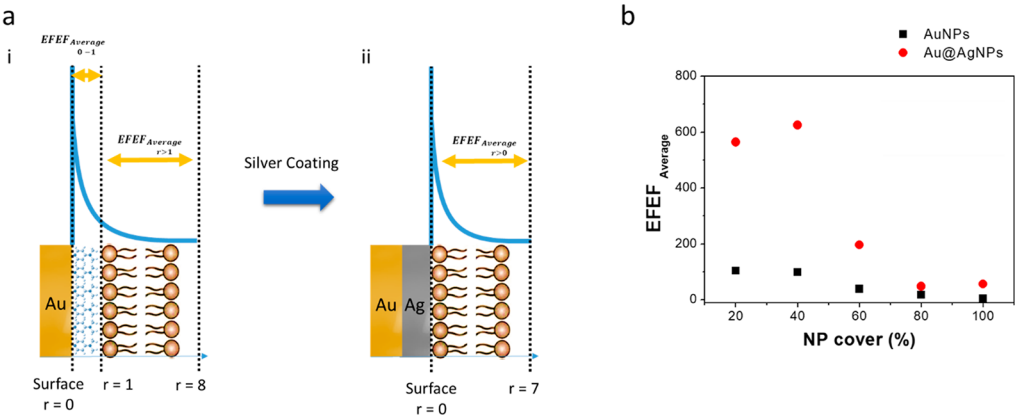

Figure 3. Theoretically expected EFEF across the ELV membrane. (a) Schematic illustration showing the colloidal SERS substrate at the ELV membrane before (i) and after the generation of a Ag layer (ii). Without Ag layer the vesicle membrane is separated from the AuNP surface by the DMAP coating, implying a lower EFEF across the ELV membrane, which is located between 1 and 8 nm from the nanoparticle surface ($EFEF_{Average/r>1}$). After applying a Ag coating, the metal surface is in direct contact with the ELV membrane, leading to a higher average EFEF across the ELV membrane, which is now positioned between 0 and 7 nm from the nanoparticle surface ($EFEF_{Average/r>0}$). (b) Theoretically expected average EFEF across the vesicle membrane is shown at 785 nm as a function of nanoparticle coverage density before ($EFEF_{Average/r>1}$) and after chemical modification ($EFEF_{Average/r>0}$) with a silver layer.

acetate for 10 s and air-dried for 24 h before imaging on the transmission electron microscope

Computational Methods. The Mie theory, which constitutes an exact solution to the problem of absorption and scattering of light by an object composed by concentric spheres,[31] was employed to simulate the optical properties of the functionalized vesicles. In particular, we used the generalized multiparticle Mie theory (GMM) formulation developed by Xu.[32] This valuable method is a suitable and rigorous formulation of the scattering problem able to exactly solve the complex problem of interaction between an electromagnetic field and an aggregate of spheres and was used to simulate the extinction, scattering, and absorption cross sections of a vesicle of 120 nm completely covered with 10 nm AuNPs with an interparticle distance of 1.3 nm, corresponding to 2 times the length of the coating agent DMAP (DMAP length = 0.65 nm). The wavelength-dependent complex refractive indices for Au and Ag were obtained from the literature.[33] As the GMM code is restricted to applications in homogeneous media, we used an effective medium approximation[34] to account for the interface between the vesicle surface and the aqueous environment. We consider that particles were immersed in a dielectric environment with an effective refractive index of n_{eff} = 1.35, which was calculated as 20% of the refractive index of the membrane (n_r = 1.45) and 80% of water (n_r = 1.33).

We also studied the local electric field enhancement distribution around each NP for both DMAP−AuNP and Au@AgNPs covering (in different percentages) a vesicle of 120 at 785 nm as irradiation wavelength (the same wavelength used for the SERS experiments). We used the GMM-FIELD code[35] to compute the electromagnetic field enhancement factor (EFEF). We obtained information about different EFEFs according to the description of the system (see Figure 2A). For computing the average EFEF over a particular region, we spatially selected the region of interest in the calculation by a maximum and minimum limit on the calculated values (Γ_{max} and Γ_{min}). The calculation was performed for different cross sections through the vesicle as shown in Figure 2A. In all the calculations the direction of the incident wave-vector *k* is parallel to the *z*-axis. For the core−shell systems, under the quasi-static approximation, the effective permittivity at 785 nm was calculated as previously described based in Maxwell−Garnett effective medium theory.[34,36]

DOI: 10.1021/acsami.9b11473
ACS Appl. Mater. Interfaces XXXX, XXX, XXX−XXX

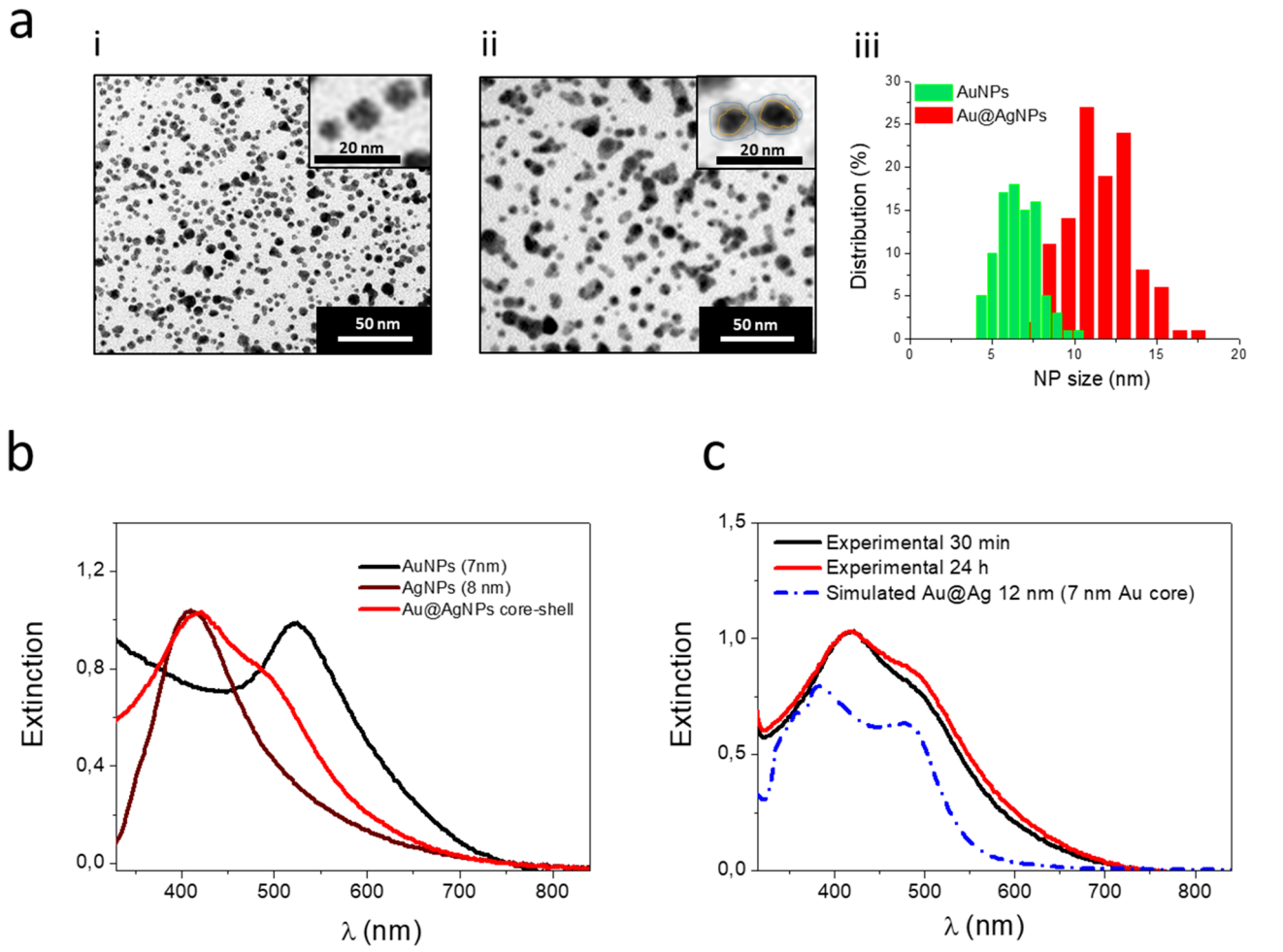

Figure 4. Generation of Au@AgNPs. (a) TEM image of AuNPs prior (i) and after formation of Au@AgNPs (ii) and size distribution determined by TEM analysis (iii). (b) Experimental extinction spectra of DMAP−AuNPs of 7 nm (AuNPs); AgNPs generated by direct mixing of silver sulfate and ascorbic acid (AgNPs); Au@AgNPs generated by adding silver sulfate and ascorbic acid to a colloidal dispersion of Au seeds. (c) Extinction spectrum of the Au@AgNPs after 30 and 24 h of the addition of the silver sulfate and ascorbic acid and simulated extinction spectrum of Au@AgNPs (12 nm = 7 nm core + 2.5 nm shell).

RESULTS

Simulations of the SERS Response of DMAP−AuNP-Coated and Au@AgNP-Coated ELVs. We started with evaluating the proposed concept from a theoretical point of view. The SERS intensity (I_{SERS}) is directly related to the electromagnetic field enhancement factor (EFEF) according to

$$I_{SERS} = F_S \sigma_S C_{SERS} \mathrm{EFEF} \quad (1)$$

where F_S is an instrumental factor, σ_S is the Raman cross section of a particular molecule, and C_{SERS} is the concentration of those molecules. Assuming small Raman shifts, EFEF scales with the fourth power of the electric field enhancement $E(\omega)/E_0(\omega)$:

$$\mathrm{EFEF} = |\Gamma(\omega)|^2 \quad (2)$$

$$|\Gamma(\omega)| = \left(\left| \frac{E(\omega)}{E_0(\omega)} \right| \right)^2 \quad (3)$$

where $|\Gamma(\omega)|$ is the square of the enhanced electric field at the frequency ω of the incident radiation.[15,37−39] To theoretically predict the expected improvement in SERS intensity of the here-proposed Au@AgNP SERS substrate compared to the previously used AuNPs functionalized with DMAP molecules (DMAP−AuNP), we performed simulations of the electric field enhancement for both types of particles attached to a vesicle of 120 nm in diameter, which is the modal diameter of B16F10-derived ELVs.[13] As DMAP is a rigid molecule with a length of 0.65 nm, close packing of particles on the vesicle surface was considered with an average interparticle distance of 1.3 nm. Figure 2a shows the spatial distribution of NPs considered in our simulations, in which the plotted points correspond to the AuNP center positions. Note that the distribution includes more than a single layer of particles in agreement with previous TEM characterization of DMAP−AuNP-coated B16F10 ELVs.[13] For calculation of the near-field response each plane has to be calculated separately. As an example, Figure 2b shows the electric field enhancement at 785 nm for the middle plane of the ELV. The distribution pattern reveals that the interparticle regions where the DMAP molecules are located (blue dashed line in zoom-in image) are preferentially excited rather than the vesicle surface.

This can also be explicitly seen in Figure 3a, where the electromagnetic EFEF is plotted in function of the radial distance from the AuNP surface. We calculated the average EFEF over a distance from 0 to 1 nm from the AuNP surface,

DOI: 10.1021/acsami.9b11473
ACS Appl. Mater. Interfaces XXXX, XXX, XXX−XXX

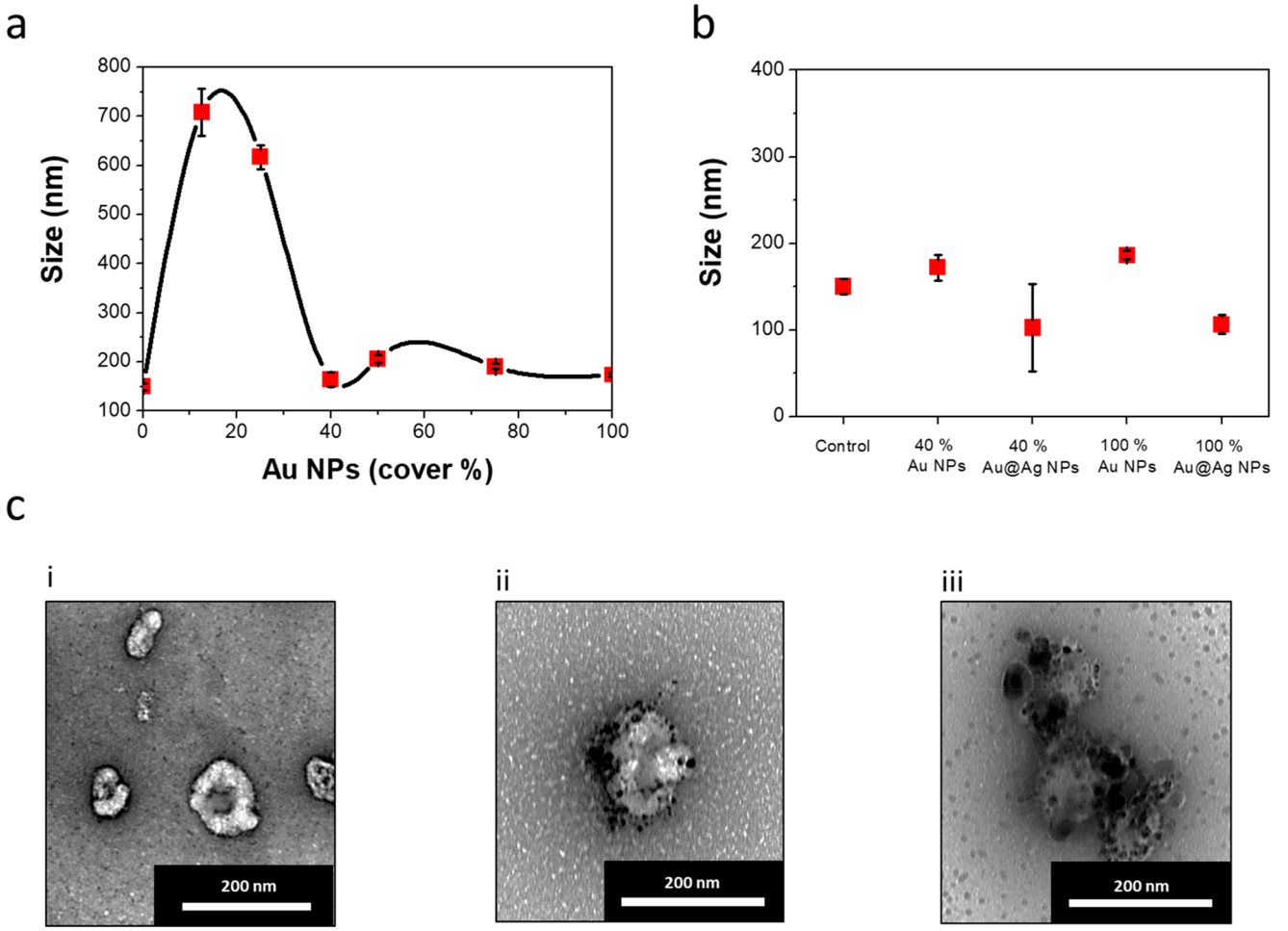

Figure 5. Generation of Au@AgNPs *in situ* over AuNP-functionalized ELVs. (a) DLS measurements of the colloidal stability of B16F10 melanoma ELVs for increasing coverage of the ELV surface with DMAP−AuNP. Error bars represent the standard deviation on the mean value (n = 3). (b) Before and after the generation of the silver layer for 40% and 100% AuNP coverage. (c) Representative TEM images of (i) B16F10 melanoma ELVs and (ii) ELVs with 40% AuNPs coverage before and (iii) after the generation of the silver layer.

which is where the DMAP molecules are located, finding an enhancement value of 4.1 × 10^5. Instead, the average EFEF from 1 to 8 nm from the AuNP surface, where the vesicle membrane is located, amounted to only 4.3, which is 9.5 × 10^4 times less (Figure 3a). The reason behind this difference in the average EFEF is related to the fact that the DMAP molecules are located in the interparticle region of the NPs. As the simulations show that the maximum near-field enhancement is located in the gaps between optically excited plasmonic NPs (the so-called hot spots), it is no surprise that the DMAP molecules experience higher enhancement factors than the molecules located at the surface or inner core of the ELVs. The EFEF distribution pattern reveals that the interparticle regions where the DMAP molecules are located are preferentially excited, while low enhancements are reached at the surface and the outer fraction of the lumen of the ELVs. This, in combination with the high Raman cross-section of DMAP, explains why these molecules contributed so strongly to the ELV SERS spectra in the original study (cf. Figure 1a).[13]

By first coating the ELVs with DMAP−AuNP and then overgrowing them with a silver layer *in situ*, we expect direct contact of the plasmonic Au@AgNP with the vesicle surface instead of the DMAP coating (Figure 3a(ii)). In that case, the average EFEF over the vesicle surface is substantially higher as for DMAP−AuNPs, as shown in Figure 2b for different nanoparticle densities at the vesicle surface (100% corresponds to full coverage assuming close packing with an interparticle distance of 1.3 nm). The best enhancement is seen at a coverage of 40%, for which the generation of a silver coating (Au@AgNPs) increases the average EFEF by 6.9 times. At higher coverage of the ELV surface the enhancement drops again due to plasmon coupling between the nanoparticles, i.e., trapping the enhanced field between the particles rather than letting it extend to the ELV membrane.

Optical Characterization of DMAP−AuNP- and Ag@AuNP-Coated ELVs. According to the theoretical simulations, the generation of a silver layer onto the already attached AuNPs is expected to substantially increase the SERS signals of the ELVs. As a next step, therefore we investigated whether it is indeed possible to generate such a silver coating onto AuNP-functionalized ELVs while maintaining an intact and colloidal stable ELV suspension. We first verified successful formation of Au@Ag core−shell particles in colloidal dispersion (i.e., without ELVs present). The chemical modification was performed according to Samal et al. by gradual reduction of Ag^+ ions using ascorbic acid (AA) as reducing agent at room temperature.[26] Figure 4a shows TEM images of the AuNPs before and after the formation of an additional silver layer. The AuNP are originally 7 ± 3 nm and become 12 ± 4 nm after formation of the silver layer, indicating an average shell

DOI: 10.1021/acsami.9b11473
ACS Appl. Mater. Interfaces XXXX, XXX, XXX−XXX

thickness of 2.5 nm. Figure 4b shows the extinction spectrum of a colloidal dispersion of DMAP-functionalized AuNPs (DMAP−AuNPs) and the spectrum obtained 30 min after the addition of silver sulfate and AA. As a reference, the spectrum of AgNPs obtained by direct mixing of silver sulfate and AA is shown as well, which had a size of 8 ± 2 nm (Figure S1). The extinction spectrum of the Au@Ag core−shell system clearly differs from the initial spectrum of both the AuNPs and AgNPs. In agreement with previous reports, the generation of the Ag coating resulted in a strong blue-shift and attenuation of the main AuNP LSPR (from 522 to 490 nm) with the appearance of Ag-like optical properties (band around 418 nm).[26,40] Figure 4c shows the spectrum 30 min and 24 h after the addition of the silver sulfate and ascorbic acid, confirming that after 30 min no further chemical modifications occurred. Also shown is the simulated spectrum of Au@AgNP which captures the main features of the experimental UV−vis spectrum quite well.

The next step was to generate the silver coating onto DMAP−AuNPs after they had been attached to the surface of B16F10 melanoma cell-derived ELVs (B16F10). This implies an additional challenge, as the reactants should not alter the ELV colloidal stability. We first evaluated the colloidal stability of ELVs mixed with different ratios of DMAP−AuNPs. Figure 5a shows the *z*-average vesicle diameter obtained by DLS as a function of the AuNP/vesicle ratio, showing that a colloidal stable system is obtained starting from a coverage of 35% (calculated as previously published),[13] which also corresponds to a complete inversion of the zeta potential to positive values. Exemplary TEM images of ELVs before and after functionalization with DMAP−AuNPs (for 40% coverage) are shown in Figures 5c(i) and 5c(ii). Next, we tested the effect of overgrowing the ELV attached DMAP−AuNP with a silver layer for two AuNP/vesicle coverage ratios, i.e., 40% and 100%, respectively. As shown in Figure 5b, applying the silver coating did not change the size appreciably, clearly indicating that it did not interfere with colloidal stability. TEM images show that the particles are still present at the ELV surface after generation of the Ag layer. To show that these particles are not caused by reduction of Ag^+ ions to Ag^0 by the biomolecules present at the ELV surface, a control experiment was performed where ELVs are mixed with an Ag^+ solution but without AA as a reducing agent. UV−vis confirmed that the reducing agent is required to generate the formation of the AgNPs (Figure S2), showing that reduction of Ag^+ is not spontaneously induced by the ELV biomolecules.

Comparison of the SERS Response of DMAP−AuNP- and Ag@AuNP-Coated ELVs. Next, we experimentally compared the SERS response of individual B16F10 melanoma ELVs coated with DMAP−AuNPs and Au@AgNPs. According to the theoretical simulations, we considered the condition of 40% coverage of the ELV surface with those nanoparticles. In addition, we included 100% coverage with DMAP−AuNP as a reference, which was the system in our previous work.[13] As can be seen in the representative spectra in Figure 6, the DMAP signals are prominently present in the SERS spectra from DMAP−AuNP-coated ELVs (blue arrows). Instead, in accordance with our hypothesis, applying an extra silver layer on the surface of the DMAP−AuNPs removed the DMAP signal and generated a "clean ELV fingerprint". The gain in EFEF for four characteristic ELV bands (red bands in Figure 6) after applying the silver coating was calculated according to

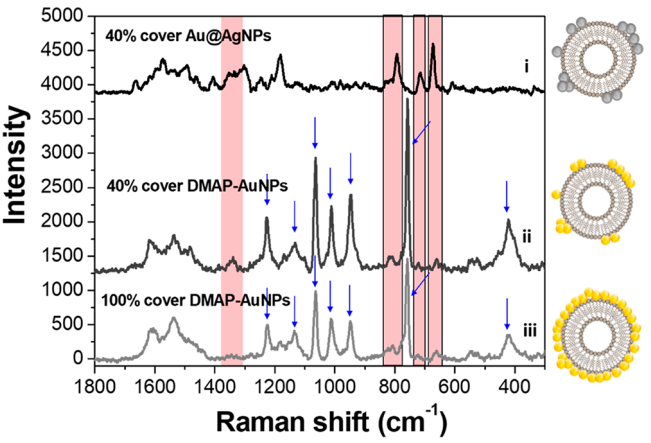

Figure 6. SERS characterization of ELVs coated with Au@AgNPs or DMAP−AuNPs. Experimental SERS spectra of B16F10 melanoma ELVs for (i) 40% coverage with Au@AgNPs, (ii) 40% coverage with DMAP−AuNPs, and (iii) 100% coverage with DMAP−AuNPs. The blue arrows indicate the most intense Raman-active modes of DMAP, which are prominently present in both (ii) and (iii) but not in (i). The spectra shown are the average of 10 individual ELV spectra.

$$\text{experimental gain} = \frac{\text{band area (40\% Au@AgNPs)}}{\text{band area (40\% DMAP−AuNPs)}} \quad (4)$$

As shown in Table 1, the average experimental gain was 5.1 ± 1.6, which is close to the theoretically expected ideal gain of 6.9.

Table 1. Theoretical and Experimental Enhancement Gains[a]

ratio 40% Au@Ag NPs/40% DMAP−AuNPs		
theoretical	EFEF average	6.9
experimental	1339−1300 cm^{-1}	4.2
	811−793 cm^{-1}	4.9
	722−715 cm^{-1}	7.4
	673−660 cm^{-1}	3.8
	average	5.1 ± 1.6

[a]Effective band area for different Raman modes in the experimental conditions (specified in Figure 5) and the GMM theoretical simulations of $EFEF_{average}$ for irradiation at 785 nm of a 120 nm vesicle covered with NPs.

Identification of Individual ELVs by SERS Spectral Analysis. To evaluate the detection capabilities of the new approach, we proceeded to measure the SERS spectra of ELVs derived from B16F10 melanoma cells (B16F10) and from red blood cells (RBC). These cell types were selected as a proof of concept to demonstrate that cancerous ELVs can be discriminated from RBC ELVs which will be present in high quantities in patient blood samples. For these experiments we selected a 40% particle coverage, as described above. Spectra were recorded from individual ELVs sedimented on a CaF_2 coverslip (Figure 7a). Figures 7b and 7c show representative SERS spectra for both ELVs (B16F10 and RBC) coated with 40% DMAP−AuNPs and 40% Au@AgNPs. As already noted above, because of the Ag coating much cleaner SERS spectra are obtained, allowing clear identification of biomolecules present in the ELV membrane. Table 2 gives an overview of identified biomolecules, assigned by comparison with already

DOI: 10.1021/acsami.9b11473
ACS Appl. Mater. Interfaces XXXX, XXX, XXX−XXX

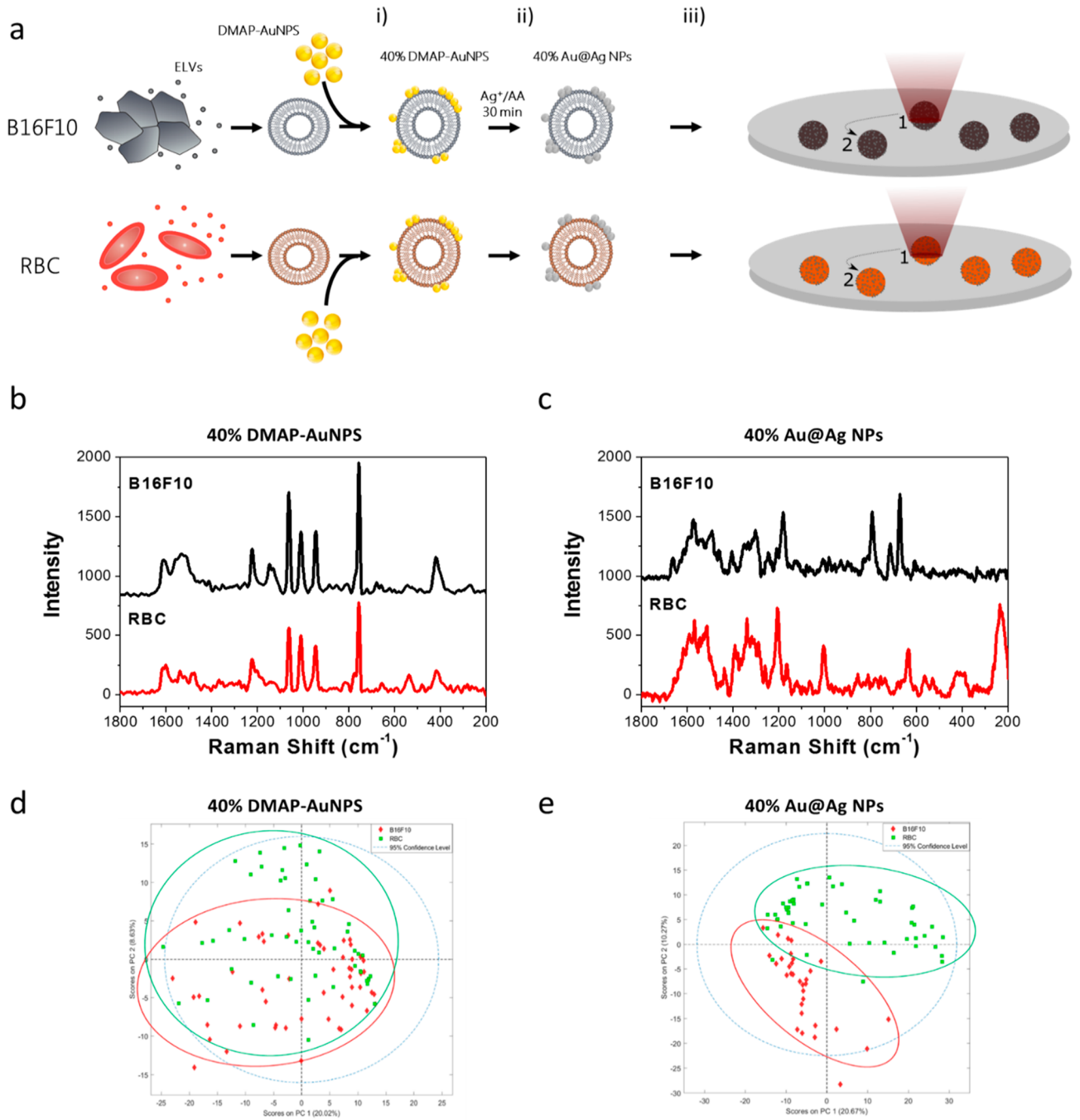

Figure 7. Discriminating different types of ELV functionalized with DMAP−AuNP and Au@AgNP. (A) Schematic representation of the procedure: (i) ELVs from B16F10 melanoma cells or RBCs are electrostatically coated with DMAP-AuNPs (40% coverage); (ii) *in situ* functionalization with a silver layer around the ELV-attached DMAP−AuNPs; (iii) SERS spectra of individual ELVs deposited on a CaF_2 coverslip are recorded with a confocal Raman microscope. Exemplary SERS spectra of individual B16F10 melanoma- and RBC-derived ELVs are shown in panels b and c, respectively. The spectra represent the average of at least 10 spectra measured over the same single vesicle. The 2D principal component analysis (PCA) for B16F10 and RBC ELVs DMAP−AuNPs and Au@AgNPs is shown in panels d and e, respectively. The indicated ellipsoids comprise 95% of the data points for each ELV type.

reported vibrational modes.[28] Thanks to the clean fingerprint with the Au@AgNP, more vibrational modes could be identified for these types of ELVs as compared with our previous study (i.e., amide bands I and II and DNA/RNA related vibrational modes).

The increase in molecular information that is obtained using the new coating strategy translates into a better separation of the B16F10 ELV and the RBC ELV data points when running an unsupervised principal component analysis (PCA) (Figure 7d,e). This minimal overlap between the two clouds of data points (Figure 7e) indicates that the variation present in the total set of recorded Raman spectra using the Au@AgNP coating strategy is mainly the result of a difference in ELV cell source. This is in contrast to the originally used DMAP−AuNP strategy for which clearly also other factors contributed to the variation in recorded spectra.[13] This further demonstrates the added value of this new coating approach for SERS-based discriminative analyses.

DOI: 10.1021/acsami.9b11473
ACS Appl. Mater. Interfaces XXXX, XXX, XXX−XXX

Table 2. Enumeration and Tentative Assignment of SERS Vibrational Modes for B16F10- and RBC-Derived ELVs Using the Au@AgNPs Core−Shell Approach

	40% Au@AgNPs[a]			
Raman shift (cm^{-1})	B16F10	RBC	previously identified in isolated ELVs	assignment of the vibrational modes[b,25]
406		m		cholesterol
521	w	m	ref 13	S−S stretching (proteins)
546	w	m	ref 13	cholesterol
645	w	s	ref 21	C−C twisting Tyr
668	s	sh		T, G (DNA/RNA)
707	m	sh	ref 21	amino acid
786	s	w	ref 21	nucleic acid
1000		s	refs 21, 22, 20	Phe
1179	s	m	ref 21	ν(C−C) and ν(C−O) (phospholipids)
1211	m	s	ref 21	Tyr, Phe
1243	m	sh	refs 13, 22	amide III (proteins)/ asymmetric phosphate stretching (nucleic acids)
1307	m	sh	refs 13, 21, 22	C−N asymmetric stretching (protein)/CH_3CH_2 twisting (lipid)
1326	m	s	refs 13, 21	ωCH_3CH_2 twisting (nucleic acids)
1381	sh	s	ref 13	δCH_3 symmetric (lipids)
1411	m	m	ref 13	
1465	w	sh	refs 13, 21	lipids
1490	s	sh	ref 20	DNA
1542	m	m	ref 22	amide II (proteins)
1563	s	s	ref 13	Trp
1592	sh	s	ref 22	
1618	sh	sh	ref 13	ν(C=C) (proteins)
1632	sh	sh		amide I α-helix and β-structure (proteins)
1664	m	sh		amide I (proteins)/DNA

[a]s: strong; m: medium; w: weak; sh: shoulder. [b]ν: vibration; δ: deformation; ω: wagging; T: thymine; G: guanine; Tyr: tyrosine; Phe: phenylalanine; Trp: tryptophan.

The final step was to investigate and quantify whether the Au@AgNP coating indeed allowed more reliable classification of individual ELVs compared to the DMAP−AuNPs. To quantify the discriminative power of the developed system, a partial least-squares discriminant analysis (PLS-DA) model was trained by SERS spectra obtained from DMAP−AuNP- or Au@AgNPs-coated ELVs from B16F10 melanoma cells and RBCs (Table 3). The specificity and sensitivity of the model were determined by cross-validation (Venetian Blinds option in PLS_Toolbox). A sensitivity of 68.6% and 83.3% and a specificity of 83.3% and 68.6% for 40% DMAP−AuNP-coated B16F10 ELVs and RBC ELVs were obtained, respectively. Instead, with Au@Ag core−shell NPs the sensitivity and specificity were always above 90% for both types of ELVs, confirming the superiority of this system.

DISCUSSION

There is a general trend in the field of ELV-based diagnostics to develop label-free strategies. In this context, several SERS substrates with different degrees of discriminative power have been previously suggested.[41] Park et al. recently reported a plasmonic SERS substrate using a carpet of AuNPs on which the ELVs can be deposited. The authors demonstrated that this substrate has the capability of discriminating ELVs derived from lung carcinoma cell lines and primary human pulmonary alveolar epithelial cells.[12] Another approach was described by Lee et al. using Ag-coated "nanobowls" for identification of SKOV3-derived ELVs.[21] Although both substrates succeeded for the identification and discrimination of ELVs, neither of these demonstrated SERS characterization at a single exosome level. The latter is important from a diagnostic point of view as the ultimate goal is to enable detection of low abundant subpopulations of ELVs from different origins in body fluids containing complex mixtures of ELVs.

Recently, we presented a simple but promising approach to achieve single ELV identification by SERS. We demonstrated that ELVs can be functionalized with DMAP stabilized AuNPs by electrostatic interaction while maintaining the colloidal stability of the ELV dispersion. While different types of individual ELVs could be successfully discriminated from one another, one of the main drawbacks of this approach was that the signal from the DMAP stabilizer was higher than the signals of the ELV biomolecules. Even though one can suggest the possibility of using other types of surface ligands with a lower Raman cross section than DMAP to increase the signal ratio between the ELV biomolecules and the AuNPs surface ligands, the simulations that we performed in this study revealed that the maximum near-field enhancement is located in the gaps between optically excited plasmonic NPs, rather than the ELV membrane (Figure 2a). As DMAP molecules are located in the interparticle region of the NPs, it is no surprise that they contribute the strongest to the SERS spectrum, thus effectively hiding much of the intrinsic ELV information that is needed to reliably determine their identity. This is also valid for other type of ligands, as they will be located at the regions of highest near-field enhancements. To overcome this limitation, here we proposed *in situ* chemical modification of ELV attached DMAP−AuNPs by generating an additional silver layer to form Au@Ag core−shell nanoparticles at the ELV surface. Not only will this silver layer remove interference of the DMAP molecules from the SERS spectra, in addition it will generate higher SERS intensities due to the plasmonic properties of a core−shell system as shown by Samal et al.[26] The former is important for correct ELV identification, while

Table 3. Comparison of the PLS-DA Classification of the Spectra of B16F10 and RBC Derived ELVs between the Previously Reported Method (AuNPs) and the Here Presented New Approach (Au@AgNPs)

			PLS-DA prediction			
SERS substrate	sample	*n*	correct identification	wrong identification	sensitivity (%)	specificity (%)
40% DMAP−AuNPs	B16F10	35	24	11	68.8	83.3
	RBC	36	30	6	83.3	68.6
40% Au@AgNPs	B16F10	12	11	1	91.7	96.9
	RBC	32	31	1	96.9	91.7

DOI: 10.1021/acsami.9b11473
ACS Appl. Mater. Interfaces XXXX, XXX, XXX−XXX

the latter allows to reduce the measurement time, which is of interest for high-throughput single ELV identification.

Theoretical simulations confirmed higher enhancements for the Au@AgNP in agreement with literature.[26] In addition, the simulations indicated that 40% coverage of the ELV surface provides the highest enhancement. This is in agreement with previous studies demonstrating that for a fixed irradiation wavelength, and for a given metal the EFEF decreases with the clusterization degree of plasmonic NPs until it reaches an almost constant value.[15] This effect is due to a combination of intrinsic damping (determined by the imaginary part of the dielectric constant of the metal at the chosen excitation wavelength) and extrinsic size effects, i.e., the radiation damping mechanism which increases with the volume of the whole cluster. Indeed, for a given metal, by increase of the aggregate size, the amount of radiation scattered by the system increases and thus the energy available to create EFEF hot spots decreases.[15]

We next evaluated whether the Ag layer could be applied without affecting the colloidal stability of the ELVs. DLS measurements and TEM images confirmed that the chemical modification had no significant effect on the colloidal stability of the ELVs (see Figure 5). Upon analysis of SERS spectra of individual ELVs, it could be confirmed that the chemical modification (Au@AgNPs) allows to remove the DMAP molecules from the Au surface so they no longer contribute to the SERS spectra (Figure 6). The exact mechanism behind this removal is still unclear, but we hypothesize that the higher affinity of the silver atoms to the Au surface displaces the physisorbed DMAP molecules, similar to what was observed for the displacement of covalently attached molecules from AuNP by sodium borohydride.[42] The effect of having cleaner SERS spectra became readily apparent when trying to discriminate ELVs derived from B16F10 melanoma cells and ELVs from red blood cells. With the Au@AgNPs a sensitivity and specificity >90% were obtained, which is a marked improvement over the DMAP−AuNPs for which a sensitivity and specificity of only 60−80% were found. In addition, 40% coverage with Au@AgNPs showed higher enhancements as theoretically predicted, reducing the integration time by 20-fold over our previously reported system of 100% surface coverage with DMAP−AuNPs. This is an important step forward since single ELV analysis requires high throughput to detect small subpopulations of interest in the large pool of isolated ELV from patient samples.

As a next step toward implementation into a diagnostic context, it will be of interest to verify whether this SERS-based technology with modified coating approach can discriminate between ELVs generated by more related parent cells such as, for example, ELVs released by primary melanocytes and cancerous melanoma cells. We are, however, hopeful as previous reports covering Raman spectroscopy and SERS measurements on bulk vesicles have shown the potential to discriminate between vesicles from very similar parent cell types[20] as well as from the same parent cell type cultured under altered environmental conditions.[22]

CONCLUSIONS

In previous work, we demonstrated that the identification of individual ELVs derived from different cell types is feasible by SERS after functionalization with AuNPs. Despite the fact that we were able to demonstrate the feasibility of single ELV identification, the quality of the SERS spectra was substantially limited by the intense signal coming from the AuNP coating agent needed for colloidal stability and attachment to the ELV surface. Here, we markedly improved this colloidal strategy for identification of individual ELVs by applying an extra silver layer *in situ* to remove interfering signals generated by the AuNP coating that is required for colloidal stability and binding to the ELV surface. This Au@AgNPs core−shell system allowed us to detect more subtle differences in the molecular composition and consequently to more reliably identify the origin of individual ELVs. In addition, the higher enhancement fields generated by the core−shell system allowed to decrease the acquisition time by a factor 20. This is critical for future diagnostic implementation as it is to be expected that disease-related ELVs have low abundance relative to those from healthy cells when analyzing patient biofluids. Moreover, this strategy preserves the simplicity and high-throughput potential of a self-assembling SERS substrate around individual ELVs. We envision that this approach can be combined with microfluidics for automated and fast SERS measurements. These features will help to overcome the technological challenge of upscaling this technology for future clinical applications.

ASSOCIATED CONTENT

Supporting Information

The Supporting Information is available free of charge on the ACS Publications website at DOI: 10.1021/acsami.9b11473.

Figures S1 and S2; supplementary methods (PDF)

AUTHOR INFORMATION

Corresponding Author

*E-mail kevin.braeckmans@ugent.be.

ORCID

Juan C. Fraire: 0000-0002-4887-2161
Andre G. Skirtach: 0000-0002-4468-7620
Stefaan De Smedt: 0000-0002-8653-2598

Author Contributions

J.C.F. and S.S. contributed equally to this work.

Notes

The authors declare no competing financial interest.

ACKNOWLEDGMENTS

This research was funded by European Research Council (ERC) under the European Union's Horizon 2020 research and innovation program (grant agreement 648214) and the Industrial Research Fund (IOF) (grant agreement F2016/IOF-ConcepTT/310). A.G.S. thanks BOF UGent (BOF14/IOP/003, BAS094-18, and 01IO3618) and FWO (G043219) for support.

REFERENCES

(1) Raposo, G.; Stoorvogel, W. Extracellular Vesicles: Exosomes, Microvesicles, and Friends. *J. Cell Biol.* **2013**, *200*, 373−383.

(2) Skog, J.; Wurdinger, T.; van Rijn, S.; Meijer, D. H.; Gainche, L.; Curry, W. T.; Carter, B. S.; Krichevsky, A. M.; Breakefield, X. O. Glioblastoma Microvesicles Transport RNA and Protein That Promote Promote Tumor Growth and Provide Diagnostic Biomarkers Johan. *Nat. Cell Biol.* **2008**, *10* (12), 1470−1476.

(3) Anastasiadou, E.; Slack, F. J. Malicious Exosomes. *Science (Washington, DC, U. S.)* **2014**, *346* (6216), 1459−1460.

DOI: 10.1021/acsami.9b11473
ACS Appl. Mater. Interfaces XXXX, XXX, XXX−XXX

(4) Zhao, L.; Liu, W.; Xiao, J.; Cao, B. The Role of Exosomes and "Exosomal Shuttle MicroRNA" in Tumorigenesis and Drug Resistance. *Cancer Lett.* **2015**, *356* (2), 339−346.
(5) Liu, C.; Xu, X.; Li, B.; Situ, B.; Pan, W.; Hu, Y.; An, T.; Yao, S.; Zheng, L. Single-Exosome-Counting Immunoassays for Cancer Diagnostics. *Nano Lett.* **2018**, *18*, 4226−4232.
(6) Ziaei, P.; Berkman, E.; Norton, M. G. Review: Isolation and Detection of Tumor-Derived Extracellular Vesicles. *ACS Appl. Nano Mater.* **2018**, *1*, 2004−2020.
(7) Wang, W.; Luo, J.; Wang, S. *Recent Progress in Isolation and Detection of Extracellular Vesicles for Cancer Diagnostics*, 2018; 1800484, 1−27.
(8) Liu, Z.; Bao, Y.; Li, B.; Sun, X.; Wang, L. Extracellular Vesicles as Circulating Cancer Biomarkers: Opportunities and Challenges. *Clin. Transl. Med.* **2018**, *7*, 1−14.
(9) Wu, A. Y.; Ueda, K.; Lai, C. P. *Proteomic Analysis of Extracellular Vesicles for Cancer Diagnostics*, 2019; 1800162, 1−12.
(10) Yamashita, T.; Kamada, H.; Kanasaki, S.; Maeda, Y.; Nagano, K.; Abe, Y.; Inoue, M.; Yoshioka, Y.; Tsutsumi, Y.; Katayama, S.; Inoue, M.; Tsunoda, S. Epidermal Growth Factor Receptor Localized to Exosome Membranes as a Possible Biomarker for Lung Cancer Diagnosis. *Pharmazie* **2013**, *68*, 969−973.
(11) Im, H.; Shao, H.; Park, Y. I.; Peterson, V. M.; Castro, C. M.; Weissleder, R.; Lee, H. Label-Free Detection and Molecular Profiling of Exosomes with a Nano-Plasmonic Sensor. *Nat. Biotechnol.* **2014**, *32*, 490−495.
(12) Park, J.; Hwang, M.; Choi, B.; Jeong, H.; Jung, J. H.; Kim, H. K.; Hong, S.; Park, J. H.; Choi, Y. Exosome Classification by Pattern Analysis of Surface-Enhanced Raman Spectroscopy Data for Lung Cancer Diagnosis. *Anal. Chem.* **2017**, *89* (12), 6695−6701.
(13) Stremersch, S.; Marro, M.; Pinchasik, B.-E.; Baatsen, P.; Hendrix, A.; De Smedt, S. C.; Loza-Alvarez, P.; Skirtach, A. G.; Raemdonck, K.; Braeckmans, K. Identification of Individual Exosome-Like Vesicles by Surface Enhanced Raman Spectroscopy. *Small* **2016**, *12* (24), 3292−3301.
(14) Tian, Y. F.; Ning, C. F.; He, F.; Yin, B. C.; Ye, B. C. Highly Sensitive Detection of Exosomes by SERS Using Gold Nanostar@ Raman Reporter@nanoshell Structures Modified with a Bivalent Cholesterol-Labeled DNA Anchor. *Analyst* **2018**, *143* (20), 4915−4922.
(15) Fraire, J. C.; Perez, L. A.; Coronado, E. A. Cluster Size Effects in the Surface-Enhanced Raman Scattering Response of Ag and Au Nanoparticle Aggregates: Experimental and Theoretical Insight. *J. Phys. Chem. C* **2013**, *117* (44), 23090−23107.
(16) Fraire, J. C.; Coronado, E. A. Design of Plasmonic Probes through Bioconjugation and Their Applications in Biomedicine: From Cellular Imaging to Cancer Therapy. In *Nanobiomaterials in Medical Imaging*; Elsevier Inc.: 2016; pp 131−162.
(17) Le Ru, E. C.; Etchegoin, P. G. Single-Molecule Surface-Enhanced Raman Spectroscopy. *Annu. Rev. Phys. Chem.* **2012**, *63* (1), 65−87.
(18) Shin, H.; Jeong, H.; Park, J.; Hong, S.; Choi, Y. Correlation between Cancerous Exosomes and Protein Markers Based on Surface-Enhanced Raman Spectroscopy (SERS) and Principal Component Analysis (PCA). *ACS Sensors* **2018**, *3* (12), 2637−2643.
(19) Kwizera, E. A.; O'Connor, R.; Vinduska, V.; Williams, M.; Butch, E. R.; Snyder, S. E.; Chen, X.; Huang, X. Molecular Detection and Analysis of Exosomes Using Surface-Enhanced Raman Scattering Gold Nanorods and a Miniaturized Device. *Theranostics* **2018**, *8* (10), 2722−2738.
(20) Tirinato, L.; Gentile, F.; Di Mascolo, D.; Coluccio, M. L.; Das, G.; Liberale, C.; Pullano, S. A.; Perozziello, G.; Francardi, M.; Accardo, A.; De Angelis, F.; Candeloro, P.; Di Fabrizio, E. SERS Analysis on Exosomes Using Super-Hydrophobic Surfaces. *Microelectron. Eng.* **2012**, *97*, 337−340.
(21) Lee, C.; Carney, R. P.; Hazari, S.; Smith, Z. J.; Knudson, A.; Robertson, C. S.; Lam, K. S.; Wachsmann-Hogiu, S. 3D Plasmonic Nanobowl Platform for the Study of Exosomes in Solution. *Nanoscale* **2015**, *7* (20), 9290−9297.
(22) Tatischeff, I.; Larquet, E.; Falcón-pérez, J. M.; Turpin, P.; Kruglik, S. G.; Tatischeff, I.; Larquet, E.; Falcón-pérez, J. M.; Turpin, P. Fast Characterisation of Cell-Derived Extracellular Vesicles by Nanoparticles Tracking Analysis, Cryo-Electron Microscopy, and Raman Tweezers Microspectroscopy. *J. Extracell. Vesicles* **2012**, *1*, 19179.
(23) Zheng, X. S.; Jahn, I. J.; Weber, K.; Cialla-May, D.; Popp, J. Label-Free SERS in Biological and Biomedical Applications: Recent Progress, Current Challenges and Opportunities. Spectrochim. *Spectrochim. Acta, Part A* **2018**, *197*, 56−77.
(24) Lane, L. A.; Qian, X.; Nie, S. SERS Nanoparticles in Medicine: From Label-Free Detection to Spectroscopic Tagging. *Chem. Rev.* **2015**, *115* (19), 10489−10529.
(25) Gittins, D. I.; Caruso, F. Spontaneous Phase Transfer of Nanoparticulate Metals from Organic to Aqueous Media. *Angew. Chem., Int. Ed.* **2001**, *40*, 3001−3004.
(26) Samal, A. K.; Polavarapu, L.; Rodal-Cedeira, S.; Liz-Marzán, L. M.; Pérez-Juste, J.; Pastoriza-Santos, I. Size Tunable Au@Ag Core-Shell Nanoparticles: Synthesis and Surface-Enhanced Raman Scattering Properties. *Langmuir* **2013**, *29* (48), 15076−15082.
(27) Vader, P.; Sachini, N.; Oirschot, B. A.; Van; Andringa, G.; Rasmussen, J. T.; Wijk, R.; Van; Solinge, W. W.; Van; Schiffelers, R. M. Taxol®-Induced Phosphatidylserine Exposure and Microvesicle Formation in Red Blood Cells Is Mediated by Its Vehicle Cremophor® EL. *Nanomedicine* **2013**, *8*, 1127−1135.
(28) Stremersch, S.; Vandenbroucke, R. E.; Van Wonterghem, E.; Hendrix, A.; De Smedt, S. C.; Raemdonck, K. Comparing Exosome-like Vesicles with Liposomes for the Functional Cellular Delivery of Small RNAs. *J. Controlled Release* **2016**, *232*, 51−61.
(29) Stremersch, S.; Brans, T.; Braeckmans, K.; De Smedt, S.; Raemdonck, K. Nucleic Acid Loading and Fluorescent Labeling of Isolated Extracellular Vesicles Requires Adequate Purification. *Int. J. Pharm.* **2018**, *548* (2), 783−792.
(30) Movasaghi, Z.; Rehman, S.; Rehman, I. U. Raman Spectroscopy of Biological Tissues. *Appl. Spectrosc. Rev.* **2007**, *42* (5), 493−541.
(31) Kang, J. W.; So, P. T. C.; Dasari, R. R.; Lim, D. High Resolution Live Cell Raman Imaging Using Subcellular Organelle-Targeting SERS-Sensitive Gold Nanoparticles with Highly Narrow Intra-Nanogap. *Nano Lett.* **2015**, *15*, 1766−1772.
(32) Marro, M.; Nieva, C.; Sanz-pamplona, R.; Sierra, A. Molecular Monitoring of Epithelial-to-Mesenchymal Transition in Breast Cancer Cells by Means of Raman Spectroscopy. *Biochim. Biophys. Acta, Mol. Cell Res.* **2014**, *1843* (9), 1785−1795.
(33) Bohrem, C. F.; Huffman, D. R. *Absorption and Scattering of Light by Small Particles*; Wiley-Interscience: New York, 1983.
(34) Xu, Y.; Wang, R. T. Electromagnetic Scattering by an Aggregate of Spheres: Theoretical and Experimental Study of the Amplitude Scattering Matrix. *Phys. Rev. E: Stat. Phys., Plasmas, Fluids, Relat. Interdiscip. Top.* **1998**, *58*, 3931−3948.
(35) Palik, E. *Handbook of Optical Constants of Solids*; Academic Press: New York, 1985.
(36) Chettiar, U. K.; Engheta, N. Internal Homogenization: Effective Permittivity of a Coated Sphere. *Opt. Express* **2012**, *20* (21), 22976−22986.
(37) Encina, E. R.; Coronado, E. A. Near Field Enhancement in Ag Au Nanospheres Heterodimers. *J. Phys. Chem. C* **2011**, *115* (32), 15908−15914.
(38) Widayanti; Abraha, K. Study on the Effect of Nanoparticle Bimetallic Coreshell Au-Ag for Sensitivity Enhancement of Biosensor Based on Surface Plasmon Resonance. *J. Phys. Conf. Ser.* **2016**, *694* (012075), 1−5.
(39) Fraire, J. C.; Masseroni, M. L.; Jausoro, I.; Perassi, E. M.; Diaz Anel, A. M.; Coronado, E. A. Identification, Localization, and Quantification of Neuronal Cell Membrane Receptors with Plasmonic Probes: Role of Protein Kinase D1 in Their Distribution. *ACS Nano* **2014**, *8* (9), 8942−8958.
(40) Fraire, J. C.; Perez, L. A.; Coronado, E. A. Rational Design of Plasmonic Nanostructures for Biomolecular Detection: Interplay

DOI: 10.1021/acsami.9b11473
ACS Appl. Mater. Interfaces XXXX, XXX, XXX−XXX

between Theory and Experiments. *ACS Nano* **2012**, *6* (4), 3441−3452.
(41) Fraire, J. C.; Sueldo Ocello, V. N.; Allende, L. G.; Veglia, A. V.; Coronado, E. A. Toward the Design of Highly Stable Small Colloidal SERS Substrates with Supramolecular Host-Guest Interactions for Ultrasensitive Detection. *J. Phys. Chem. C* **2015**, *119* (16), 8876−8888.
(42) Li, Y.; Shi, Q.; Zhang, P.; Xiahou, Y.; Li, S.; Wang, D.; Xia, H. Empirical Structural Design of Core @ Shell Au @ Ag Nanoparticles for SERS Applications. *J. Mater. Chem. C* **2016**, *4*, 6649−6656.
(43) Merdalimova, A.; Chernyshev, V.; Nozdriukhin, D.; Rudakovskaya, P.; Gorin, D.; Yashchenok, A. Identification and Analysis of Exosomes by Surface-Enhanced Raman Spectroscopy. *Appl. Sci.* **2019**, *9*, 1135.
(44) Ansar, S. M.; Ameer, F. S.; Hu, W.; Zou, S.; Pittman, C. U.; Zhang, D. Removal of Molecular Adsorbates on Gold Nanoparticles Using Sodium Borohydride in Water. *Nano Lett.* **2013**, *13* (3), 1226−1229.

DOI: 10.1021/acsami.9b11473
ACS Appl. Mater. Interfaces XXXX, XXX, XXX−XXX